

Original scientific paper

Mucoadhesive Polymer Hyaluronan as Biodegradable Cationic/Zwitterionic-Drug Delivery Vehicle

Francisco Torrens✉ and Gloria Castellano¹

Institut Universitari de Ciència Molecular, Universitat de València, Edifici d'Instituts de Paterna, P. O. Box 22085, E-46071 València, Spain

¹Facultad de Veterinaria y Ciencias Experimentales, Universidad Católica de Valencia San Vicente Mártir, Guillem de Castro 94, E-46001 València, Spain

✉Corresponding Author: E-mail: torrens@uv.es; Tel.: +34-963-544-431; Fax: +34-963-543-274

Received: July 23, 2014; Revised: August 28, 2014; Published: January 09, 2015

Abstract

Mucoadhesive polymers in pharmaceutical formulations release drugs in mucosal areas. They interact and fix to mucus through molecular interpenetration, etc., which increase drug bioavailability. Polymers physicochemical properties affect formulation mucoadhesion, rheological behaviour and drug absorption. Hyaluronan (HA) is selected as a mucoadhesive and biodegradable polymer. Geometric, topological and fractal analyses are carried out with program TOPO. Reference calculations are performed with algorithm GEPOL. Procedure TOPO underestimates molecular volume by 0.7 %. The error results 5 % in surface area and derived topological indices. The solvent-accessible surface is undercalculated by 3 %: from hexamer HA to HA·3Ca and hydrate, the hydrophobic term rises by 42% and decays by 26 %, as well as the hydrophilic part drops by 14% and rises by 58 %, in agreement with the number of H-bonds. The accessibility rises by 9 % and decays by 8 %. The fractal dimension is underevaluated by 1 % and, for HA, it results 1.566; on going to HA·3Ca and hydrate, it rises by 2 % and 1 %. The nonburied-atoms dimension increases by 11 %: for HA, it results 1.725. When going to HA·3Ca and hydrate, it augments by 4 % and 0.3%. Ongoing from HA to HA·3Ca and hydrate, the external minus molecular dimension enlarges by 20 % and decays by 9 %. The hydrate globularity is lower than for water, Ca²⁺ and averages of O-atoms in HA. The rugosity of Ca²⁺ is smaller than for hydrate, averages of O-atoms in HA and water. The accessibilities of Ca²⁺ and water are greater than for hydrate. As cations exchange in HA·3Ca requires Ca²⁺ alteration, rises of drug zwitterionic character and acidic pH increase absorption.

Keywords

medicine absorption; medicine delivery; dipole moment; fractal dimension; metal hyaluronate; mucosa.

Introduction

Hyaluronic acid (HA) is a high-molecular-weight (MW) (HMW) polysaccharide present in the extracellular matrix of most vertebrate tissues [1]. Its functions vary from maintaining constant volume of interstitial fluid to organizing extracellular matrix and immunosuppression [2]. Its presence on plasma membranes and concentration variation in pericellular spaces are associated with cell aggregation during morphogenesis and metastasis formation during malignant transformation and tumours invasion [3–5]. It is an anionic, nonsulphated, linear, HMW polyglycosaminoglycan (*cf.* Figure 1) consisting of repeating units

of disaccharide D-glucuronic acid (GCU)- $\beta(1\rightarrow3)$ -N-acetyl-D-glucosamine (NAG)- $\beta(1\rightarrow4)$. An HA molecule consists of 10^4 GCU/NAG. Its anionic charge under physiological conditions is caused by GCU COO^- , which M^{2+} interaction contributes to global supramolecular structure [6]. Other factors include: pH, temperature, hydration and, especially, M^{2+} [7,8]. Structural and literature data for transition metal complexes with HA are limited to aqueous co-ordination complexes with Ca^{2+} , Ag^+ , Cd^{2+} , Pb^{2+} and Fe^{3+} [9–11]. X-ray fibre diffraction solved solid-state structure of M^{2+} HA where the formation of 2- and 4-fold-helices was reported [12–15]. Polyanion conformation is stabilized by *H-bonds* across glycosidic linkages between HA monomers. Adjacent antiparallel chains are held together through $\text{COO}^- \text{Ca}^{2+} \text{OOC}^-$ bridges and six *H-bonded* water molecules. The polymer secondary structure is similar to Ca^{2+} HA for other M^{2+} . Amorphous M^{2+} HA ($\text{M} = \text{Cu}, \text{Ni}, \text{Mn}, \text{Co}$) was prepared at pH 5.5 precipitating aqueous solutions with cold ethanol. Local structure around M^{2+} was determined by extended X-ray absorption fine structure (EXAFS) and X-ray absorption near edge structure (XANES) [16,17]. Co-ordination polyhedron around Cu^{2+} is a distorted octahedron: four O-atoms at a distance of 1.95 Å occupy planar equatorial sites; at axial places O-atoms are present at 2.46 Å. Though O-atoms are preferred at axial locations, N-atoms from NAG cannot be excluded.

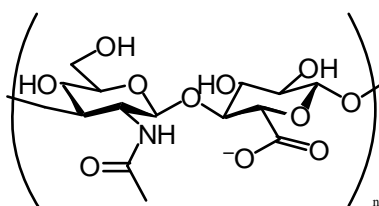


Figure 1. Disaccharide repeating unit of HA comprising GCU/NAG. The MW ranges in 10^4 – 10^7 $\text{g}\cdot\text{mol}^{-1}$.

By using quantum chemical methods, the basic GCU/NAG unit was studied. Semi-empirical and *ab initio* molecular orbital (MO) calculations showed optimized geometries in agreement with crystallographic data [18]. The Ca/Cu^{2+} HA are amorphous materials. A combined quantum mechanical/molecular mechanics (QM/MM) approach [19] to enzymology and M^{2+} -protein/HA binding allowed structural elucidation [20–28]. Transition- M^{2+} binding was studied by using density-functional theory (DFT) [29–33]. An HA: Ca/Cu^{2+} -complexation QM/MM was performed [34]. The HA plays a structural role in cartilage and other tissues. Aggrecan, the cartilage proteoglycan, is bound to HA chains, the bond being stabilized by link proteins [35]. The formed aggregates of $\text{MW} \sim 10^8 \text{g}\cdot\text{mol}^{-1}$ are deposited within the collagen framework, without which interaction the proteoglycans would not be retained in cartilage. Mucoadhesive polymers were used in pharmaceutical formulations to release drugs in mucosas [gastrointestinal (GI)/vaginal tracts, ocular mucosa, bucal/nasal cavity] [36]. They fix to mucus through mechanisms (molecular interpenetration, van der Waals forces, hydrophobic interactions, electrostatic forces, *H-bonds*) increasing drug bioavailability [37–40].

In earlier publications, program TOPO was applied to the valence topological charge-transfer indices for the molecular dipole moment [41,42], as well as fractal dimension of percutaneous absorption enhancer phenyl alcohols [43] and 4-alkylanilines [44]. Lysozyme showed hydrolytic activity vs. peptidoglycans [45–48]. A new tool was described for interrogating macromolecular structure [49]. In the present report, HA geometric, topological and fractal analyses are performed with TOPO. The aim of this study is to find properties distinguishing $\text{HA}\cdot 3\text{Ca}\cdot 9\text{H}_2\text{O}$. The goal is to validate the indices by using HA differentiation. The ultimate reason for modelling is to improve pharmaceutical formulations to release drugs in mucosal areas as HA properties affect mucoadhesion, rheological behaviour and drug absorption with the goal of increasing biodisponibility and decreasing toxicity. The following section describes the experimental *in*

silico computational methods. Next, two sections illustrate and discuss the results. Finally, the last section summarizes our conclusions.

Experimental

In our program TOPO for the theoretical simulation of crystal-fragment shape [50], structure surface is represented by the external surface of a set of overlapping spheres with appropriate radii, centred on the atomic nuclei [51,52]. A crystal fragment is treated as a solid in space defined by tracing spheres about atomic nuclei. It is computationally enclosed in a graduated rectangular box, and the geometric descriptors are evaluated by counting the points within the solid or close to chosen surfaces. The crystal-fragment volume is approximated as $V = P \cdot \text{GRID}^3$, where P is the number of points within the fragment volume (within a distance R_x of any atomic nucleus X) and GRID is the mesh-grid size. As a first approximation, the crystal-fragment *bare* surface area was calculated as $S = Q \cdot \text{GRID}^2$, where Q is the number of points close to the *bare* surface area (within a distance between R_x and $R_x + \text{GRID}$ of any atomic nucleus X). However, the estimate was improved: if a point falls exactly on the surface of one of the atomic spheres it accounts indeed for GRID^2 units of area on fragment *bare* surface, which is because total surface of atom X can accommodate $4\pi R_x^2 / \text{GRID}^2$ points. When a point falls beyond the surface it represents GRID^2 units of area on the surface of a sphere of radius $R > R_x$, not on the surface of atom X on which it accounts only for a fraction of this quantity: $\text{GRID}^2 (R_x/R)^2$. The total *bare* surface area is calculated as $S = F \cdot \text{GRID}^2$, where F is the sum of elements $AF = R_x^2 / R^2(I)$ for those points close enough to the surface of any atom X . The R_x^2 is the square radius of atom X and $R^2(I)$ is the square distance of point I from atomic nucleus X . Two topological indices of crystal-fragment shape are calculated: $G = S_e/S$ (S_e = surface of an equivalent sphere) stands for the fragment globularity and $G' = S/V$ denotes the fragment *rugosity*.

The hydrated-system properties are related to the contact surface between solute and water molecules. Another crystal-fragment geometric descriptor was proposed: the *solvent-accessible surface* area AS [53], which is defined by using a probe sphere that is allowed to roll on the outside while maintaining contact with the *bare* surface [54]. It is calculated in the same way as the bare surface area by using pseudo-atoms whose van der Waals radii [55] were increased by the probe radius R [56]. The *accessibility* is a dimensionless quantity ranged in 0–1 representing the ratio of solvent-accessible surface area in a particular structure to solvent-accessible surface area of the same atom when isolated from the crystal-fragment. The *fractal dimension*, D , results [57]:

$$D = 2 - \frac{d(\log AS)}{d(\log R)} \quad (1)$$

It provides a quantitative indication of the degree of surface accessibility towards different solvents [58]. Program TOPO allows an atom-to-atom analysis of D on every atom i to obtain an atomic dimension index D_i from the atomic contributions to AS_i . The D_i is weight averaged to obtain a new crystal-fragment dimension index $D' = (\sum_i AS_i D_i) / AS$, where AS_i are used as weights for D_i . If an $AS_i = 0$ for any probe, D_i cannot be calculated for atom i and this does not contribute to D' , which represents a D averaged for atoms *nonburied* to any solvent-accessible surface in the range of probe spheres. A version of TOPO was implemented in algorithms AMYR [59], GEPOL [60] and SURMO2 [61]. Procedure AMYR performs the theoretical simulation of molecular associations and chemical reactions. Software GEPOL performs a

triangular tessellation of the crystal-fragment surface. It is used for reference calculations. Codes TOPO and GEPOL recognize the cavity-like spaces in crystal-fragments and are adequate to study intercalation compounds; however, SURMO2 does not distinguish internal cavities. Combination SURMO2 with TOPO or GEPOL allows characterizing the crystal-fragment surface of the cavities. Our version of SURMO2 was corrected for deviation from the spherical shape, by dividing the contribution of every point by the cosine of the angle formed by the semi-axis and the corresponding normal vector to the surface at this point. The volume and surface areas of the crystal fragments with cavities were corrected by maximizing in every angular orientation the distance of the most distant atom in each semi-axis.

Calculation Results

Doubly crosslinked networks (DXNs) were engineered by embedding gelatine conjugated HA hydrogel particles (HGP) (gHGPs) in a secondary net established by HA glycidyl methacrylate (GMA) (HAGMA) (*cf.* Figure 2) [62].

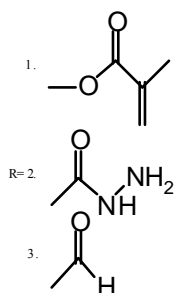


Figure 2. Chemical modifications in synthetic procedures for the fabrication of HA HGPs and DXNs.

For drug administration on mucous membranes and tissues, as well as skin, the active principle is prepared in matrix systems with a hydrophilic polymer {Carbopol[®] [poly(acrylic acid) (PAA), *cf.* Figure 3a], HA} and alcohol [propylene glycol (PG, Figure 3b), poly(ethylene glycol) (PEG, Figure 3c)].

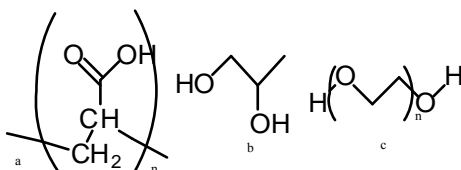


Figure 3. (a) Poly(acrylic acid) (PAA); (b) propylene glycol (PG); (c) poly(ethylene glycol) (PEG).

Fourier-transform infrared (FTIR) spectroscopy showed that the carboxylic acid groups COOH of PAA react completely with the alcohol groups OH in the matrix [63]:



In gel Ca alginate used for wound dressing, Ca^{2+} releasing helps in healing and exchanges exuded Na^+ . Stable cationic colloids were elaborated by using chitosan (CS):HA polyelectrolyte complexation [64]. $\text{Ag}^+/\text{Ag}_3\text{PO}_4$ nanoparticles:HA/CS complexes (*cf.* Figure 4) resulted antimicrobial [65,66]. Hydrogels are used in medical applications, *e.g.*, implants, tissue engineering and contact lenses.

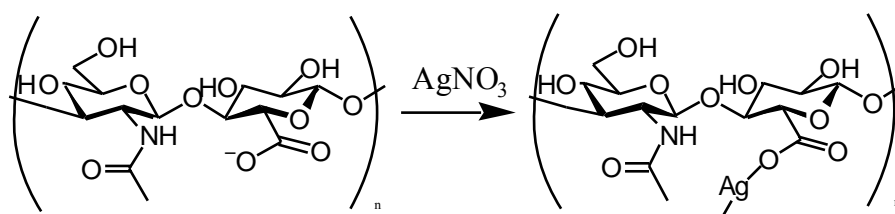


Figure 4. Suggested structure of complex of hyaluronic acid (HA) and silver Ag^+ .

The HA was selected as a mucoadhesive and biodegradable polymer. Polar molecules (*cf.* Table 1) administered with HA show high dipole moment. Notice the low MW of metronidazole, *etc.* and the low human skin permeability of caffeine used as transdermal anticellulite. Some small, lipid-soluble drugs cross the blood–brain barrier (BBB) simply by diffusion through the cell membrane and others, *e.g.*, caffeine, enter successfully through specialized transporter proteins.

A model showed that the decimal logarithm of 1-octanol–water partition coefficient ($\log P$) positively correlated and MW negatively associated with $\log K_p$ [67]:

$$\log K_p = -6.3 + 0.71 \log P - 0.006 \text{MW}, \quad n = 93 \quad r = 0.82 \quad (3)$$

where n is the number of points and r , correlation coefficient. Table 2 shows the administration routes of drug metronidazole for bacterial, fungal and protozoal vaginitis [68,69].

Table 1. Molecular dipole moments of water, theophylline and polar molecules administered with HA.

Molecule	μ (D) ^a	Ref. ^b	MW ^c	$\text{p}K_a$ ^d	$\log P$ ^e	$\log K_p$ ^f	Uses
Water	1.861	1.85	18	15.74	-1.38	-6.71	Solvent and metabolism
Eugenol	2.378	–	164	10.19	2.27	–	Local antiseptic and anaesthetic
Theophylline	3.262	–	180	8.81	-0.773	–	Respiratory diseases
Caffeine	3.567	3.64	194	10.4	-0.07	-7.14	Cellulite
Metronidazole	3.681	–	171	2.62	-0.02	–	Bacterial/fungal/protozoal vaginitis
Terconazole	4.098	–	532	<1.5	3.51	–	Antifungal
Minoxidil	4.292	–	209	4.61	1.24	–	Androgenic alopecia
Betamethasone	5.346	–	392	12.42	1.94	–	Anti-inflammatory and immunosuppressor

^a μ : Molecular dipole moment (Debye) calculated with MOPAC-AM1 [70], ^b μ : Calculated molecular dipole moment (Debye), ^cMW: molecular weight ($\text{g}\cdot\text{mol}^{-1}$), ^d K_a : Acid dissociation constant ($\text{mol}\cdot\text{L}^{-1}$), ^e P : 1-octanol–water partition coefficient, ^f K_p : human skin permeability ($\text{cm}\cdot\text{s}^{-1}$).

Table 2. Administration routes of drug metronidazole for bacterial, fungal and protozoal vaginitis.

Route	Onset	Peak (hr)	Duration (hr)
Oral (PO)	Rapid	1–3	8
PO (extended)	Rapid	Unknown	Up to 24
Intravenous (IV)	Rapid	End of infusion	6–8
Topical	Unknown	6–12	Unknown
Vaginal	Unknown	6–12	12

An HA comparative analysis was performed in three forms: hexamer (trimer of heterodimers) HA (*cf.* Figure 5), HA-3Ca and HA-3Ca·9H₂O. The geometry of the systems was taken from the Protein Data Bank code 4HYA (X-ray fibre diffraction).

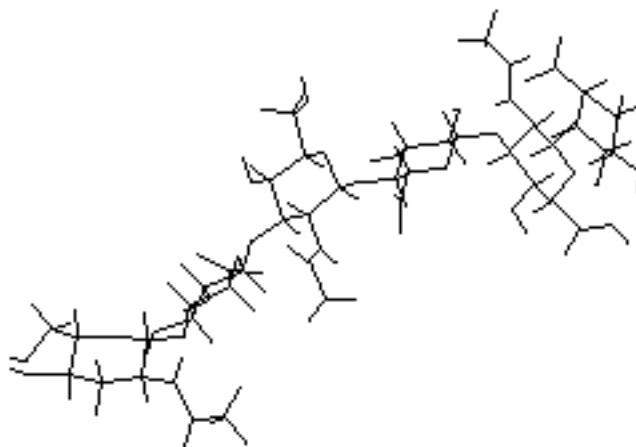


Figure 5. Wire-frame molecular structure of HA (perspective view).

In 4HYA, nine crystallization water molecules are included most strongly bound in the first hydration shell (*cf.* Figure 6).

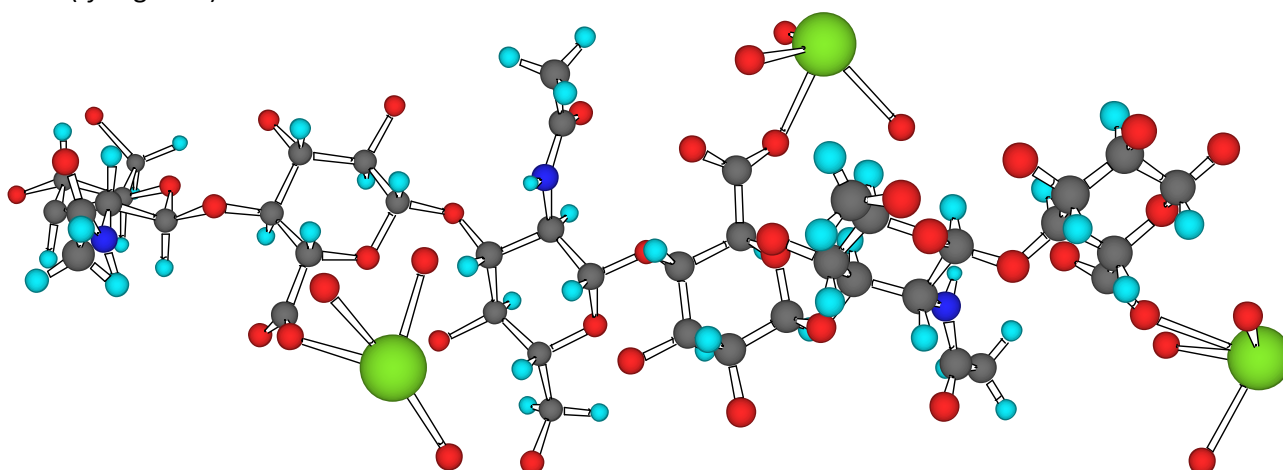


Figure 6. Hydrogen-suppressed ball-and-stick structure of hyaluronic acid hexamer HA·3Ca·9H₂O.

The 4HYA consists of six saccharide residues (126 atoms, *cf.* Table 3) with MW = 1123g·mol⁻¹. The glycosaminoglycan hexamer co-ordinates three Ca²⁺ ions also surrounded by at least nine water molecules. The 11 N/O–H...O *H-bonds* include one N–H...O and 10 O–H...O, *e.g.*, three pairs of H-shared *H-bonds*. Many *H-bonds* are formed because of the polyanionic nature of HA main chain.

Table 3. Number of atoms, hydrogen bonds and molecular weight of hyaluronic acid (HA).

Molecule	No. of Atoms	MW (g·mol ⁻¹) ^a	Number of N/O–H...O Hydrogen Bonds
HA	126	1123	1 N–H...O
HA·3Ca	129	1243	1 N–H...O
HA·3Ca·9H ₂ O	152	1401	11 (1 N–H...O + 10 O–H...O, 6 shared)

^a MW: Molecular weight (g·mol⁻¹).

Figure 7 illustrates four out of 11 N/O–H...O *H-bonds* in HA·3Ca·9H₂O: one N–H...O and three out of 10 O–H...O.

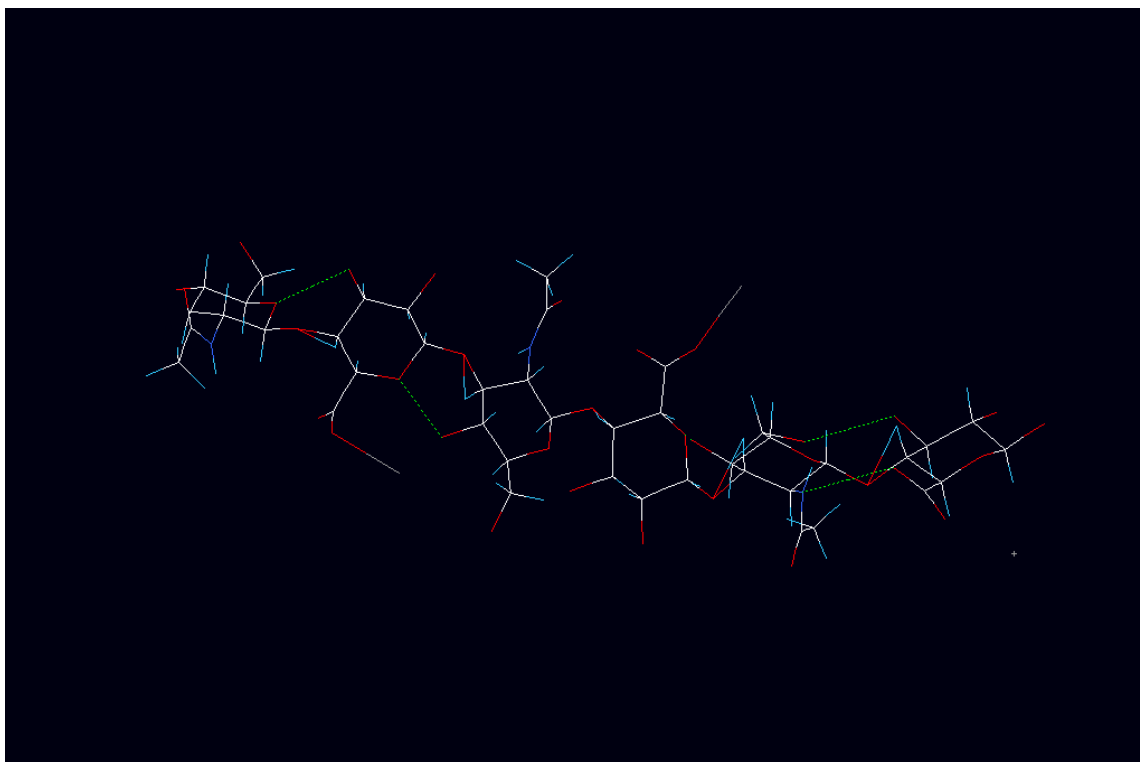


Figure 7. Four of the N/O–H...O hydrogen bonds of hyaluronic acid hexamer HA·3Ca·9H₂O.

Van der Waals molecular surface of HA·3Ca·9H₂O (*cf.* Figure 8) shows some small open cavities.

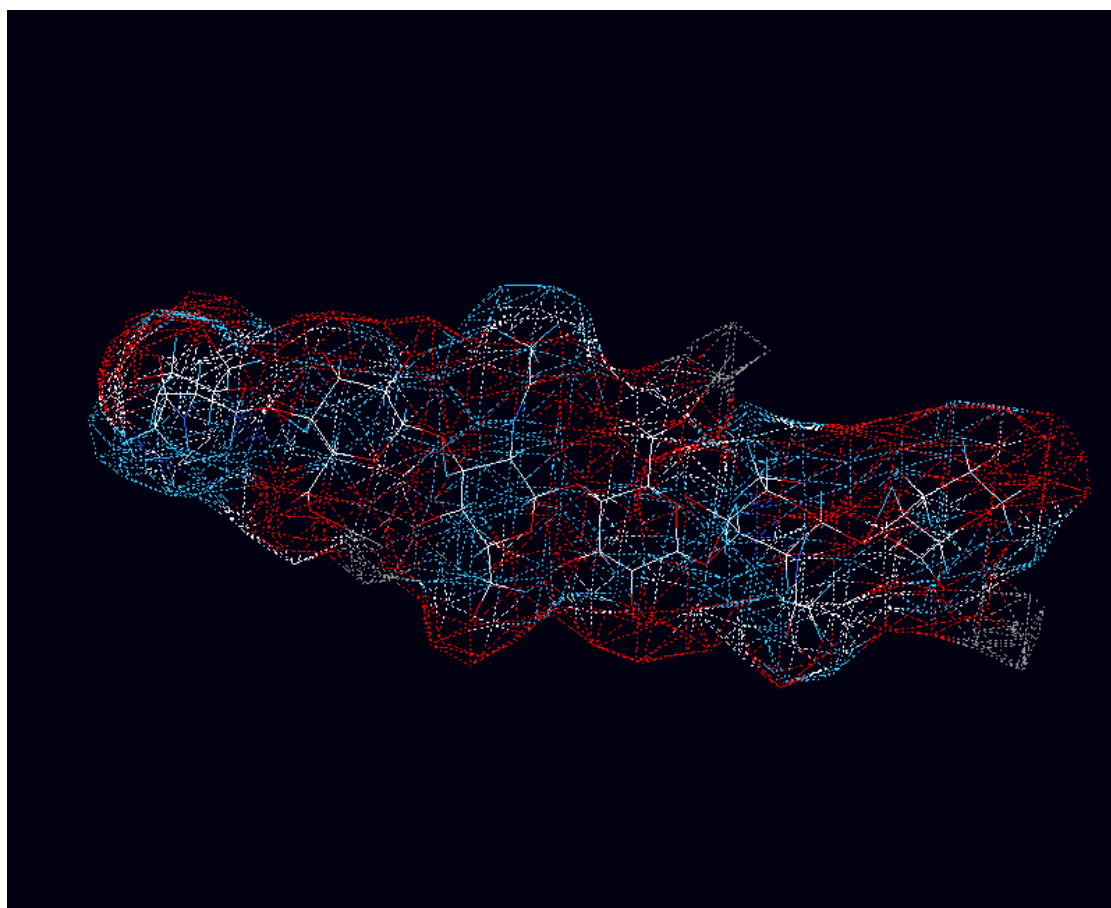


Figure 8. Van der Waals molecular surface of hyaluronic acid hexamer HA·3Ca·9H₂O.

Geometric and topological analyses were performed with our program TOPO (*cf.* Table 4). Reference calculations were performed with our version of GEPOL. Algorithm TOPO underestimated the molecular volumes V and surface areas S by 0.7% and 5 %, respectively. Surface-derived molecular globularities G were overestimated by 5% and rugosities G' resulted underestimated by 5 %.

Table 4. Geometric descriptors and topological indices of hyaluronic acid (HA).

Molecule	V^a	V Ref. ^b	S^c	S Ref. ^b	G^d	G Ref. ^b	G'^e	G' Ref. ^b
HA	816.4	822.8	942.78	999.24	0.448	0.425	1.155	1.214
HA·3Ca	913.3	919.9	1069.45	1128.66	0.426	0.405	1.171	1.227
HA·3Ca·9H ₂ O	1070.0	1077.8	1247.91	1320.73	0.405	0.385	1.166	1.225

^a Molecular volume (\AA^3), ^b Reference calculation carried out with program GEPOL, ^c Molecular surface area (\AA^2), ^d Molecular globularity, ^e Molecular rugosity (\AA^{-1}).

Figure 9a shows the wire-frame molecular structure of HA. Figure 9b reveals the ball-and-stick (B&S) molecular model of HA·3Ca·9H₂O. The Corey-Pauling-Koltun (CPK) molecular structure of HA·3Ca·9H₂O (Figure 9c) defines the van der Waals molecular surface area S . Notice some small open cavities on CPK surface in agreement with Figure 8. The water-accessible surface CPK⁺ of HA·3Ca·9H₂O (Figure 9d) delimits the solvent-accessible surface area AS. Most open cavities on CPK (Figure 9c) close on CPK⁺ surface meaning that they are not accessible to a water molecule (radius $R = 1.25 \text{\AA}$). The CPK⁺⁺ of HA·3Ca·9H₂O (Figure 9e) denotes the surface accessible by a protein side chain ($R = 3.50 \text{\AA}$) and is used to calculate the fractal dimension D . Again, most open cavities on CPK (Figure 9c) close on CPK⁺⁺, which are not accessed by a protein side chain. Structures comparison suggests that HA·3Ca·9H₂O reaction with a molecule or drug begins with water and, even, Ca²⁺ exchanges in the co-ordination compound. As many drugs are either cationic or zwitterionic, *e.g.*, 65 % of orally available drugs are charged or zwitterionic, Ca²⁺ exchange is favoured by electrostatics at acidic pH; *e.g.*, drugs metronidazole and minoxidil are ionic pairs.

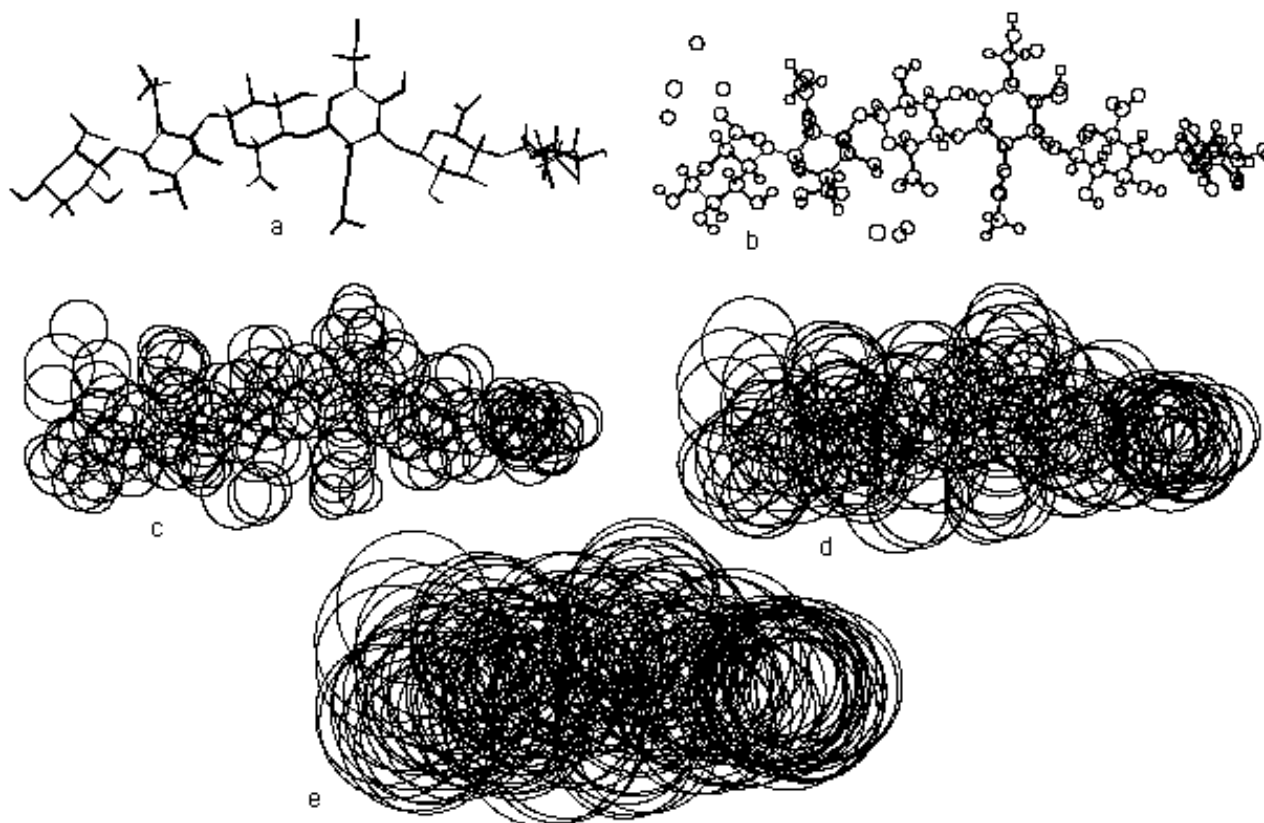


Figure 9. HA·3Ca·9H₂O molecular structures: (a) wire frame; (b) B&S; (c) CPK; (d) CPK⁺; (e) CPK⁺⁺.

Surface CPK⁺ of HA (*cf.* Figure 10) shows more open cavities than HA·3Ca·9H₂O (Figure 9d), which could be accessed by a water molecule.

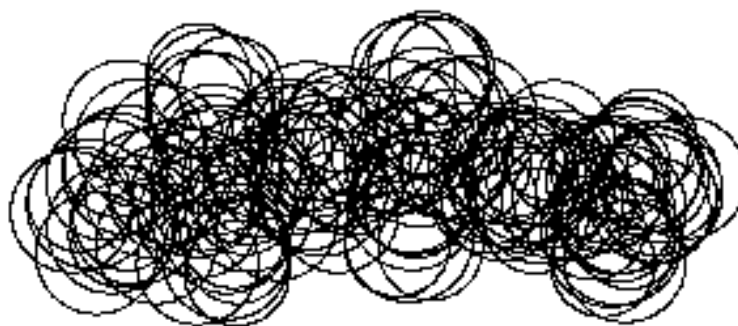


Figure 10. CPK⁺ molecular surface of HA.

Program TOPO allows the atom-to-atom partition analysis of all geometric descriptors. Water solvent-accessible surface analysis (*cf.* Table 5) shows that the solvent-accessible surface (AS) area was underestimated by 3 %. When going from hexamer HA to HA·3Ca and HA·3Ca·9H₂O the hydrophobic solvent-accessible surface (HBAS) area rose by 42% and decayed by 26 %, respectively. On the other hand, the hydrophilic solvent-accessible surface (HLAS) area dropped by 14 % and increased by 58 %. It resulted the most sensitive geometric descriptor for the presence of Ca²⁺ and, especially, water, in agreement with the highest number of *H-bonds* in the hydrated co-ordination complex (Table 3). Ongoing from HA to HA·3Ca and HA·3Ca·9H₂O, the accessibility enlarged by 9% and decreased by 8%. The fractal dimension *D* was undervalued by 1 %. The fractal dimension of HA turned out to be 1.566. When going to HA·3Ca and HA·3Ca·9H₂O, it rose by 2 % and 1 %. The low accessibility and relatively low dimension of HA·3Ca·9H₂O suggest that its reaction requires water or Ca²⁺ exchange, in agreement with the closed character of CPK^{+/++} surfaces (Figure 9). The fractal dimension averaged for *nonburied* atoms *D'* increased by 11% with regard to the molecular dimension. In particular, for HA the external dimension resulted 1.725. Ongoing to HA·3Ca and HA·3Ca·9H₂O it augmented by 4% and 0.3%. When going from HA to HA·3Ca and HA·3Ca·9H₂O, the difference nonburied minus molecular dimensions (*D'–D*) enlarged by 20 % and decayed by 9 %. It resulted greatly sensitive to Ca²⁺ and water incidences.

Table 5. Geometric descriptors and fractal dimensions of the solvent-accessible surface of HA.

Molecule	AS ^a	AS Ref. ^b	HBAS ^c	HLAS ^d	Accessibility ^e	<i>D</i> ^f	<i>D</i> Ref. ^b	<i>D'</i> ^g	<i>D'–D</i>
HA	1255.03	1293.95	589.72	665.31	11.14	1.566	1.582	1.725	0.159
HA·3Ca	1409.77	1453.85	834.57	575.20	12.09	1.601	1.619	1.792	0.191
HA·3Ca·9H ₂ O	1530.07	1578.40	620.88	909.19	11.15	1.625	1.644	1.798	0.173

^a Water solvent-accessible surface area (Å²), ^b Reference calculation carried out with program GEPOL, ^c Hydrophobic solvent-accessible surface area (Å²), ^d Hydrophilic solvent-accessible surface area (Å²), ^e Accessibility (%), ^f Molecular fractal dimension, ^g Molecular fractal dimension averaged for nonburied atoms.

Atom-to-atom partition analyses of HA·3Ca·9H₂O topological indices and fractal dimension, *cf.* Table 6, show that globularity *G* of hydrated co-ordination complex was lower than for O-atoms in water, Ca²⁺ and averages of O-atoms in HA in 2.0–2.4. Rugosity *G'* of Ca²⁺ was smaller than for hydrate, O-atom averages in HA in 1.2–1.3Å⁻¹ and O-atoms in water. Hydrate accessibility lay in the range of O-atom averages in HA (5.9–11.9%); however, accessibilities of Ca²⁺ and O-atoms in water (34%) were much greater. On the other hand, the fractal dimensions of hydrate, Ca²⁺ and O-atoms in water lay in the range of averages of O-atoms in HA (1.1–3.6). In particular, maximum fractal dimension corresponds to GCU O-atoms for which the utmost reactivity is expected, in agreement with M^{Z+}-interchange and Ag⁺ reactions (Figure 4).

Table 6. Atom-atom partition analyses of HA·3Ca·9H₂O topological indices and fractal dimension.

Fragment	G^a	G^b	Accessibility (%)	D^c
Average of O atoms in NAG ₁	2.415	1.177	11.94	1.104
Average of O atoms in GCU ₁	2.038	1.295	8.95	3.597
Average of O atoms in NAG ₂	2.067	1.290	8.11	1.710
Average of O atoms in GCU ₂	2.069	1.270	5.93	1.358
Average of O atoms in NAG ₃	2.332	1.215	9.36	2.245
Average of O atoms in GCU ₃	1.975	1.293	10.66	1.801
Average of O atoms in NAG	2.271	1.227	9.80	1.686
Average of O atoms in GCU	2.027	1.286	8.51	2.252
Average of O atoms in HA	2.138	1.259	9.10	1.995
Average of Ca ²⁺ cations	1.430	1.087	33.57	1.492
Average of O atoms in H ₂ O	1.258	1.733	33.54	1.700
HA·3Ca·9H ₂ O	0.405	1.166	11.15	1.625

^a Molecular globularity, ^b Molecular rugosity (Å⁻¹), ^c Molecular fractal dimension.

Discussion

Natural polysaccharide HA gelifies at $pH < 4$. It is characterized by its regenerative properties on different mucous zones, *e.g.*, GI, oral, vaginal, *etc.* The HA is mainly used in medical and cosmetic applications. Among the many benefits HMW-HA holds in medicine are: (1) the maintenance of tissue space for surgery, (2) protection of cells and tissue and (3) therapeutic effectiveness. Healing efficiency of HA depends critically on MW: the higher the MW, the longer its benefit. The use of HA in cosmetics presents an impact on public health because of the risk of ingredient penetration into the deeper skin layers, which are cleared by systemic circulation (systemic absorption is more likely to occur in injured skin, *e.g.*, sunburnt, atopic, eczematous, psoriatic skin). The problem is important in the case of anticellulite creams as the tissue target is on the dermis. Caffeine, *Coleus forskohlii* and *Nelumbo nucifera* extracts are efficacious ingredients of anticellulite cosmetics. In order to develop formulations, it is interesting to enhance their low skin permeabilities (Table 1). However, care should be taken concerning toxicity. Finally, it is proposed that (1) polymer COOHs react completely with matrix OHs to give esters, (2) polymer reaction with drugs begins with water or, even, Ca²⁺ exchange, (3) matrix rheological properties, *e.g.*, pH -dependent gelification, *etc.*, are important and (4) caffeine is a potential lead structure in drug design.

Conclusions

From the present results and discussion the following conclusions can be drawn:

1. The advantage of program TOPO with respect to GEPOL is that the former allows an atom-to-atom partition analysis of the geometric, topological, fractal indices and their combination: hydrophobic and hydrophilic solvent-accessible surface areas. The latter was detected as the most sensitive geometric descriptor for the presence of Ca²⁺ and, especially, water, in agreement with the number of *H-bonds*, which were calculated with TOPO. Ongoing from hyaluronan to Ca²⁺ co-ordinated to hydrate, accessibility rose by 9 % and decayed by 8 %. The relative error with program TOPO is 0.7 % in volume, as well as 5 % in surface area and its derived indices.
2. The fractal dimension was undervaluated by 1 %. Ongoing to Ca²⁺ co-ordinated and hydrate, fractal dimension of hyaluronan (1.566) rose by 2 % and 1 %, respectively. The fractal dimensions of *nonburied* atoms increased by 11 % with regard to molecular fractal indices. Ongoing to Ca²⁺ co-ordinated to hydrate, fractal dimension of external atoms (1.725) augmented by 4 % and 0.3 %. Nonburied minus molecular fractal dimension enlarged by 20 % and decayed by 9 %. It was sensitive to Ca²⁺ and water occurrences.

3. The hydrate globularity was lower than for O-atoms in water, Ca^{2+} and O-atom average in hyaluronan. The rugosity of Ca^{2+} was smaller than for hydrate, O-atoms average in hyaluronan and O(water). The accessibility of Ca^{2+} and O(water) was much greater than for hydrate. The maximum fractal dimension corresponds to D-glucuronic-acid O-atoms for which the utmost reactivity is expected, in agreement with M^{2+} interchange and Ag^+ reactions.
4. As cations exchange in hyaluronan co-ordination compound and action requires Ca^{2+} alteration, the reinforcement of drug cationic/zwitterionic character and acidic pH increases absorption. Hyaluronan is an articular-cartilage component where it is present as coat around chondrocytes. When aggrecan monomers bind to it in link-protein presence, large, anionic aggregates form, which are responsible for cartilage resilience. Its water interaction, represented by 10–15 *H-bonds* per disaccharide repeat, indicates binding capacity and importance for cartilage viscoelastic properties. In mucosas, a need for the elimination of pathogens and prophylaxis exists. The hyaluronan rheological behaviour in pH 4–7 did not differ. However, pH < 4 generated gels because of hydrophobic interactions and *H-bonds*, which resulted promising for drug administration on mucous membranes and skin.

Further work will analyze polymer reactions with alcohols in the matrix/drugs (eugenol, metronidazole, betamethasone, etc.), matrix rheological properties and caffeine as a potential lead structure in drug design. Caffeine, etc. are efficacious ingredients of anticellulite cosmetics. However, care should be taken concerning toxicity, especially for injured skin. Work is in progress on the prediction of chromatographic retention times and molecular classification of (1) tea compounds and (2) methylxanthines (caffeine and its metabolites) and nicotine-metabolite cotinine in human plasma.

Acknowledgements: F. T. thanks support from the Spanish Ministerio de Economía y Competitividad (Project No. BFU2013-41648-P) and EU ERDF.

References

- [1] E.A. Balazs, Ed., *The Chemistry and Molecular Biology of the Intercellular Matrix*, Academic, New York, NY, 1970
- [2] B. Alberts, A. Johnson, J. Lewis, M. Raff, K. Roberts, P. Walter, *Molecular Biology of the Cell*, Garland, New York, NY, 2002
- [3] T.C. Laurent, J.R.E. Fraser, *FASEB J.* **6** (1992) 2397-2404
- [4] K.L. Goa, P. Benfield, *Drugs* **47** (1994) 536-566
- [5] E. Zimmerman, B. Geiger, L. Addadi, *Biophys. J.* **82** (2002) 1848-1857
- [6] M. Moulabbi, H. Broch, L. Rober, D. Vasilescu, *J. Mol. Struct. (THEOCHEM)* **395-396** (1997) 477-508
- [7] P. Sipos, M. Veber, K. Burger, J. Illes, G. Machula, *Acta Chim. Hung. Models Chem.* **129** (1992) 671-683
- [8] E.R. Morris, D.A. Rees, E.J. Welsh, *J. Mol. Biol.* **138** (1980) 383-400
- [9] N. Figueroa, B. Nagy, B. Chakrabarti, *Biochem. Biophys. Res. Commun.* **74** (1977) 460-465
- [10] H. Sterk, M. Braun, O. Schmut, H. Feichtinger, *Carbohydr. Res.* **145** (1985) 1-11
- [11] L. Lapcik, C. Dammer, M. Valko, *Colloid Polym. Sci.* **201** (1992) 1049-1052
- [12] J.K. Sheehan, E.D. Atkins, *Int. J. Biol. Macromol.* **5** (1983) 215-221
- [13] E.D. Atkins, J.K. Sheehan, C.F. Phelps, *Biochem. J.* **128** (1972) 1255-1263
- [14] A.K. Mitra, S. Raghunathan, J.K. Sheehan, S. Arnott, *J. Mol. Biol.* **169** (1983) 829-859
- [15] W.T. Winter, S. Arnott, *J. Mol. Biol.* **117** (1977) 761-784

- [16] E. Tratar Pirc, I. Arcon, P. Bukovec, A. Kodre, *Carbohydr. Res.* **324** (2000) 275-282
- [17] E. Tratar Pirc, I. Arcon, A. Kodre, P. Bukovec, *Carbohydr. Res.* **339** (2004) 2549-2554
- [18] R. Eklund, G. Widmalm, *Carbohydr. Res.* **338** (2003) 393-398
- [19] A. Warshel, M. Levitt, *J. Mol. Biol.* **103** (1976) 227-249
- [20] B.R. Brooks, R.E. Bruccoleri, B.D. Olafson, D.J. States, S. Swaminatham, M. Karplus, *J. Comput. Chem.* **4** (1983) 187-217
- [21] A.D. Becke, *Phys. Rev. A* **38** (1988) 3098-3100
- [22] C.T. Lee, W.T. Yang, G. Parr, *Phys. Rev. B* **37** (1988) 785-789
- [23] A.D. MacKerell Jr., D. Bashford, M. Bellott, R.L. Dunbrack Jr., J.D. Evanseck, M.J. Field, S. Fischer, J. Gao, H. Guo, S. Ha, D. Joseph-McCarthy, L. Kuchnir, K. Kuczera, F.T.K. Lau, C. Mattos, S. Michnick, T. Ngo, D.T. Nguyen, B. Prodhom, W.E. Reiher III, B. Roux, M. Schlenkrich, J.C. Smith, R. Stote, J. Straub, M. Watanabe, J. Wiórkiewicz-Kuczera, D. Yin, M. Karplus, *J. Phys. Chem. B* **102** (1998) 3586-3616
- [24] E. Tratar Pirc, J. Zidar, P. Bukovec, M. Hodoscek, *Carbohydr. Res.* **340** (2005) 2064-2069
- [25] L. Masgrau, A. Roujeinikova, L.O. Johannissen, P. Hothi, J. Basran, K.E. Ranaghan, A.J. Mulholland, M.J. Sutcliffe, N.S. Scrutton, D. Leys, *Science* **312** (2006) 237-241
- [26] J. Zidar, E. Tratar Pirc, M. Hodoscek, P. Bukonec, *J. Chem. Model.* **48** (2008) 283-287
- [27] Y. Zhao, D. Truhlar, *Theor. Chem. Acc.* **120** (2008) 215-241
- [28] B.R. Brooks, C.L. Brooks III, A.D. Mackerell Jr., L. Nilsson, R.J. Petrella, B. Roux, Y. Won, G. Archontis, C. Bartels, S. Boresch, A. Caflisch, L. Caves, Q. Cui, A.R. Dinner, M. Feig, M. Fischer, J. Gao, M. Hodoscek, W. Im, K. Kuczera, T. Lazaridis, J. Ma, V. Ovchinnikov, E. Paci, R.W. Pastor, C.B. Post, J.Z. Pu, M. Schaefer, B. Tidor, R.M. Venable, H.L. Woodcock, X. Wu, W. Yang, D.M. York, M. Karplus, *J. Comput. Chem.* **30** (2009) 1545-1614
- [29] T.E. Hofstetter, C. Howder, G. Berden, J. Oomens, P.B. Armentrout, *J. Phys. Chem. B* **115** (2011) 12648-12661
- [30] M. Remko, D. Fitz, R. Broer, B.M. Rode, *J. Mol. Model.* **17** (2011) 3117-3128
- [31] M.H. Khodabandeh, R. Hamid, K. Zare, M. Zahedi, *Int. J. Mass Spectrom.* **313** (2012) 47-57
- [32] P.E. Siegbahn, *J. Biol. Inorg. Chem.* **11** (2006) 695-701
- [33] Y. Minenkov, Å. Singstad, G. Occhipinti, V.R. Jensen, *Dalton Trans.* **41** (2012) 5526-5541
- [34] E. Tratar Pirc, J. Zidar, P. Bukovec, *Int. J. Mol. Sci.* **13** (2012) 12036-12045
- [35] D. Heinegård, Å. Oldberg, *FASEB J.* **3** (1989) 2042-2051
- [36] G.S. Asane, S.A. Nirmal, K.B. Rasal, A.A. Naik, M.S. Mahadik, Y.M. Rao, *Drug Dev. Ind. Pharm.* **34** (2008) 1246-1266
- [37] N.A. Peppas, P.A. Buri, *J. Control Release* **2** (1985) 257-275
- [38] J.M. Gu, J.R. Robinson, S.H. Leung, *Crit. Rev. Ther. Drug Carrier Syst.* **5** (1988) 21-67
- [39] J. Woodley, *Clin. Pharmacokinet.* **40** (2001) 77-84
- [40] J.D. Smart, *Adv. Drug Deliv. Rev.* **57** (2005) 1556-1568
- [41] F. Torrens, *Molecules* **8** (2003) 169-185
- [42] F. Torrens, *Molecules* **9** (2004) 1222-1235
- [43] F. Torrens, *Leb. Sci. J.* **5**(1) (2004) 61-70
- [44] F. Torrens, G. Castellano, *J. Liq. Chromatogr. Relat. Technol.* **31** (2008) 2337-2347
- [45] F. Torrens, G. Castellano, A. Campos, C. Abad, *J. Mol. Struct.* **924-926** (2009) 274-284
- [46] F. Torrens, G. Castellano, *Anal. Chim. Acta* **654** (2009) 2-10
- [47] F. Torrens, G. Castellano, *J. Life Sci.* **5** (2011) 167-181
- [48] F. Torrens, G. Castellano, *Asia Pacific J. Life Sci.* **5** (2013) 89-121
- [49] F. Torrens, G. Castellano, *J. Mater. Sci. Eng. B* **4**(2) (2014) 55-63

- [50] F. Torrens, E. Ortí, J. Sánchez-Marín, *J. Chim. Phys. Phys.-Chim. Biol.* **88** (1991) 2435-2441
- [51] A.Y. Meyer, *J. Chem. Soc., Perkin Trans. 2* **1985** (1985) 1161-1169
- [52] A.Y. Meyer, *J. Comput. Chem.* **9** (1988) 18-24
- [53] B. Lee, F.M. Richards, *J. Mol. Biol.* **55** (1971) 379-400
- [54] R.B. Hermann, *J. Phys. Chem.* **76** (1972) 2754-2759
- [55] A. Bondi, *J. Phys. Chem.* **68** (1964) 441-451
- [56] S.J. Wodak, J. Janin, *Proc. Natl. Acad. Sci. U. S. A.* **77** (1980) 1736-1740
- [57] M. Lewis, D.C. Rees, *Science* **230** (1985) 1163-1165
- [58] F. Torrens, J. Sánchez-Marín, I. Nebot-Gil, *J. Comput. Chem.* **22** (2001) 477-487
- [59] F. Torrens, M. Rubio, J. Sánchez-Marín, *Comput. Phys. Commun.* **115** (1998) 87-89
- [60] J.L. Pascual-Ahuir, E. Silla, J. Tomasi, R. Bonaccorsi, *J. Comput. Chem.* **8** (1987) 778-787
- [61] B. Terryn, J. Barriol, *J. Chim. Phys. Phys.-Chim. Biol.* **78** (1981) 207-212
- [62] X. Xu, A.K. Jha, D.A. Harrington, M.C. Farach-Carson, X. Jia, *Soft Matter* **8** (2012) 3280-3294
- [63] S.A.A. Al-Abdulla, N.A.H. Al-Assady, S.G. Syyah, *J. Thi-Qar Sci.* **3** (2012) 129-140
- [64] R.C. Polexe, T. Delair, *Molecules* **18** (2013) 8563-8578
- [65] A.M. Abdel-Mohsen, R. Hrdina, L. Burget, G. Krylova, R.M. Abdel-Rahman, A. Krejcova, M. Steinhart, L. Benes, *Carbohydr. Polym.* **89** (2012) 411-422
- [66] D. Chudobova, L. Nejdil, J. Gamulec, O. Krystofova, M.A. Merlos Rodrigo, J. Kynicky, B. Ruttkay-Nedecky, P. Kopel, P. Babula, V. Adam, R. Kizek, *Int. J. Mol. Sci.* **14** (2013) 13592-13614
- [67] R.O. Potts, R.H. Guy, *Pharm. Res.* **9** (1992) 663-669
- [68] C.D. Freeman, N.E. Klutman, K.C. Lamp, *Drugs* **54** (1997) 679-708
- [69] S. Löfmark, C. Edlund, C.E. Nord, *Clin. Infect. Dis.* **50** (2010) S16-S23
- [70] M.J.S. Dewar, E.G. Zoebisch, E.F. Healy, J.J.P. Stewart, *J. Am. Chem. Soc.* **107** (1985) 3902-3909